inter.noise
HAMBURG 2016

Low frequency sound transmission of double plates in an impedance tube

Hyun-Sil KIM[1]; Jae-Seung KIM[2]; Seong-Hyun LEE[3]; Yun-Ho SEO[4]; Pyung-Sik MA[5]

Acoustics and Noise Research Team

Korea Institute of Machinery and Materials, Republic of Korea

ABSTRACT

In this paper, low frequency STL (Sound Transmission Loss) of single and double plates installed in an impedance tube is studied using an analytic method. The vibration motion of the plates and sound pressure field are expanded in terms of the infinite series of modal functions. Under the plane wave condition, the low frequency approximation is derived by including the first few symmetric modes, where anti-symmetric modes do not contribute to wave propagation. Comparison of the STL done by the proposed method with the FEM results shows an excellent agreement. It is found that the peak frequencies of the double plates coincide with those of each single plate. When the two plates are identical, the STL becomes zero at the natural frequencies of the single plate. However, when the two plates are not identical, the STL is always greater than zero. The location and amplitude of the dips are investigated using an approximate solution when the cavity depth is very small.

Keywords: Sound transmission loss, duct I-INCE Classification of Subjects Number(s): 51.4

1. INTRODUCTION

It is well known that the STL of a finite plate in the low frequency range is significantly affected by the stiffness and the boundary conditions (1). Osipov *et al.* (2) studied the STL in a room-plate-room model, and found that low frequency sound insulation depends on the geometry and the dimensions of the system. Lee and Kim (3) investigated the sound transmission characteristics of an infinite plate stiffened by equally spaced line stiffeners. They applied the space-harmonic expansion method to determine that the STL shows a dip, and as the stiffener spacing decreases, the dip moves to higher frequency, which results in a large STL in the low frequency range. Varanasi *et al.* (4) considered the STL of a small rectangular plate that comprised the single unit cell of a large periodic barrier. They studied the STL of the single plate in a standing wave tube (impedance tube) using the FEM (finite element method) and measurement, where high STL was observed in the low frequency range. Piscoya and Ochman (5) calculated the STL of thin plates in a Kundt's duct (impedance tube) using the BEM (boundary element method) in addition to measurement; they confirmed high STL in the low frequency range. Jessop *et al.* (6) used the FEM to explore the STL of a stiffened window in a standing wave tube; the effect of the stiffener location was studied. As observed in previous works (2)-(6) performed using the FEM/BEM or measurements, the STL of a finite single plate shows a dip at the lowest natural frequency, and monotonically increases as the frequency decreases below that frequency. Kim *et al*. (7) studied the STL of a single rectangular plate in an impedance tube using an analytical approach. They expanded the vibration motion of the plate and sound pressure field in terms of the infinite series of the modal functions. Under the plane wave condition, they demonstrated that only the first few modes are enough to simulate the behaviors of the plate as well as the sound field in the low frequency range.

[1] hskim@kimm.re.kr
[2] jskim@kimm.re.kr
[3] sh.lee@kimm.re.kr
[4] yhseo@kimm.re.kr
[5] psma@kimm.re.kr

The STL of finite double panels shows more complicated behavior than that of a finite single panel due to interaction among the plates and the cavity. Panneton and Atalla (8) treated finite multilayer systems with poroelastic materials using the FEM. They found that the STL has multiple dips and peaks, and monotonically increases as frequency decreases below the first dip, which is related to the plate mode. Xin *et al*. (9, 10) employed the mode expansion method to investigate sound transmission through finite double-panel partitions for simply supported condition (9) and clamped condition (10); they showed results similar to those found in reference 8.

The STL of the plates in a duct is of great importance from a practical aspect. Measurement or numerical analysis of a specimen in a duct is more manageable than the partitions between two large reverberation chambers, and yet it can still give physical insight for the design of the STL of a panel system. High STL of plates in low frequency range has wide applications in noise control problems, where low frequency noise is dominant, like HAVC (heating, air conditioning, and ventilation) noise, propeller noise in ships, and transformer noise, etc. This paper is an extension of reference (7) to the case of double plates, where the STL of thin double plates with an air cavity between them in a rigid duct is considered. The cross-section of the duct is square. The analytical solution is compared with results obtained using the FEM to confirm the accuracy of the proposed method. It is discussed how parameters such as plate thickness and cavity depth affect the STL, and how they change the dips and peaks.

2. FORMULATION OF THE STL

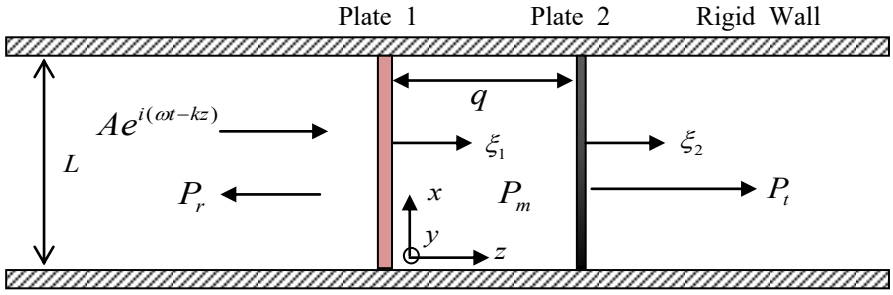

Figure 1 – Incidence of a plane wave onto the double elastic plates in a rigid duct.

We consider a rigid impedance tube in which a plane wave is incident to double thin plates, where q is the gap between plates 1 and 2. The cross-section of the duct is square, and the boundary conditions of the plates are the same. Inside the cavity, a wave is generated as

$$p_m = \sum_{r=0}^{N_r} \sum_{s=0}^{N_s} [b_{rs} e^{i(\omega t - k_z z)} + c_{rs} e^{i(\omega t + k_z z)}] \cos(\frac{\pi r x}{L}) \cos(\frac{\pi s y}{L}), \quad (1)$$

where L is the height of the plate, ω is the angular frequency, and $i = \sqrt{-1}$. Wavenumber k_z in z direction satisfies the following relation:

$$\pi^2 (r^2 + s^2)/L^2 + k_z^2 = k^2, \quad (2)$$

where $k = \omega / c$, and c is the speed of sound in the air. The summation limit N_r and N_s in Eq. (1) are determined such that k_z becomes a real number in Eq. (2).

The transmitted pressure p_t is given by

$$p_t = \sum_{r=0}^{N_r} \sum_{s=0}^{N_s} d_{rs} \cos(\frac{\pi r x}{L}) \cos(\frac{\pi s y}{L}) e^{i(\omega t - k_z z)}. \quad (3)$$

In the left-side of plate 1, a reflected wave is generated as

$$p_r = A e^{i(\omega t + k_z z)} + \sum_{r=0}^{N_r} \sum_{s=0}^{N_s} e_{rs} \cos(\frac{\pi r x}{L}) \cos(\frac{\pi s y}{L}) e^{i(\omega t + k_z z)}. \quad (4)$$

The boundary conditions at the plate surfaces are

$$\frac{1}{\rho}\frac{\partial p}{\partial z} = -\frac{\partial^2 \xi_1}{\partial t^2} = \omega^2 \xi_1 \quad \text{at} \quad z = 0, \tag{5}$$

$$\frac{1}{\rho}\frac{\partial p}{\partial z} = -\frac{\partial^2 \xi_2}{\partial t^2} = \omega^2 \xi_2 \quad \text{at} \quad z = q, \tag{6}$$

where ρ is the density of air, and $\xi_1 = \tilde{\xi}_1 e^{i\omega t}$ and $\xi_2 = \tilde{\xi}_2 e^{i\omega t}$ are the displacements of plates 1 and 2, respectively. From Eqs. (1) and (3)-(5), the relations between the coefficients are obtained as

$$e_{rs} = -b_{rs} + c_{rs} \qquad \text{at} \quad z = 0, \tag{7}$$

$$-b_{rs}e^{-ik_z q} + c_{rs}e^{ik_z q} = -d_{rs}e^{-ik_z q} \qquad \text{at} \quad z = q. \tag{8}$$

If the common term $e^{i\omega t}$ is omitted, the governing equations for the plates are given by

$$D_1 \nabla^4 \tilde{\xi}_1 - M_1 \omega^2 \tilde{\xi}_1 = 2A + \sum_{r=0}^{N_s} \sum_{s=0}^{N_s} (e_{rs} - b_{rs} - c_{rs}) \cos(\frac{\pi r x}{L}) \cos(\frac{\pi s y}{L}), \tag{9}$$

$$D_2 \nabla^4 \tilde{\xi}_2 - M_2 \omega^2 \tilde{\xi}_2 = \sum_{r=0}^{N_s} \sum_{s=0}^{N_s} (b_{rs}e^{-ik_z q} + c_{rs}e^{ik_z q} - d_{rs}e^{-ik_z q}) \cos(\frac{\pi r x}{L}) \cos(\frac{\pi s y}{L}), \tag{10}$$

where $D_j = E_j h_j^3 / 12(1-\nu_j^2)$, $M_j = \rho_{pj} h_j$, and $E_j, h_j, \nu_j, \rho_{pj}$ denote Young's modulus, thickness, Poisson's ratio and the density of the plate j $(j = 1,2)$, respectively. In Eq. (9), $2A$ denotes the blocked pressure. Structural damping is considered by introducing a complex Young's modulus $E(1+i\eta)$, where η is loss factor.

If the plates are simply supported, the displacement of the plates can be expressed as

$$\tilde{\xi}_1(x,y) = \sum_{m=1}^{\infty} \sum_{n=1}^{\infty} a_{mn} \phi_m(x) \phi_n(y), \qquad \tilde{\xi}_2(x,y) = \sum_{m=1}^{\infty} \sum_{n=1}^{\infty} T_{mn} \phi_m(x) \phi_n(y), \tag{11}$$

where $\phi_m(x) = \sin(m\pi x / L)$, and there exists natural frequency ω_{mn} corresponding to the (m,n) mode of the plate. If h is the thickness of the plate, ω_{mn} is given by

$$\omega_{mn} = \frac{\pi^2 h (m^2 + n^2)}{L^2} \sqrt{\frac{E}{12\rho_p(1-\nu^2)}}. \tag{12}$$

However, for clamped plates, displacement of the plates cannot be expressed as the product of the beam mode as in Eq. (11). In general, displacements are given by (11, 12)

$$\tilde{\xi}_1(x,y) = \sum_{j=1}^{\infty} a_j \Phi_j(x,y), \qquad \tilde{\xi}_2(x,y) = \sum_{j=1}^{\infty} T_j \Phi_j(x,y), \tag{13}$$

where $\Phi_j(x,y)$ is the j_{th} mode of the clamped plate. Although no closed form of $\Phi_j(x,y)$ for the clamped plate exists, approximate solutions are available for the first few modes. Young (11) used the products of clamped beam functions and the Rayleigh-Ritz method to compute modes and corresponding natural frequencies. He used a 36-term series as

$$\Phi_j(x,y) = \sum_{m=1}^{6} \sum_{n=1}^{6} a_{mn}^j \phi_m(x) \phi_n(y), \tag{14}$$

where $\phi_m(x)$ is the m_{th} mode of the clamped beam vibration (11,12). The natural frequency corresponding to the j_{th} mode is given by the following form

$$\omega_j = \frac{\lambda_j h}{L^2} \sqrt{\frac{E}{12\rho_p(1-\nu^2)}}. \tag{15}$$

The coefficients a_{mn}^j are tabulated in references (11)-(12), and listed in Table 1 for the first three modes, and parameter λ_j in Table 2 .

Table 1. Coefficients a_{mn}^{j} in Eq. (14) from reference (12)

Mode 1	Mode 2	Mode 3
$a_{11}=1.0000$	$a_{12}=1.0000$	$a_{22}=1.0000$
$a_{13}=0.0142$	$a_{14}=0.0101$	$a_{24}=0.0326$
$a_{15}=0.0020$	$a_{16}=0.0020$	$a_{26}=0.0073$
$a_{31}=0.0142$	$a_{32}=0.0406$	$a_{42}=0.0326$
$a_{33}=$-0.0031	$a_{34}=$-0.0022	$a_{44}=$-0.0019
$a_{35}=$-0.0009	$a_{36}=$-0.0007	$a_{46}=$-0.0010
$a_{51}=0.0020$	$a_{52}=0.0070$	$a_{62}=0.0073$
$a_{53}=$-0.0009	$a_{54}=$-0.0011	$a_{64}=$-0.0010
$a_{55}=$-0.0004	$a_{56}=$-0.0005	$a_{66}=$-0.0006

The coefficients for the mode 1 in Table 1 reveals that a_{11} is much larger than the rest of the coefficients a_{mn}, from which Φ_1 can be simplified as $\Phi_1 \approx \phi_1(x)\phi_1(y)$. Similarly, we have $\Phi_2 \approx \phi_1(x)\phi_2(y)$ and $\Phi_3 \approx \phi_2(x)\phi_2(y)$. In Table 2, simplified expressions of the mode shape are listed.

Table 2. Simplified expression of the mode shape $\Phi_j(x,y)$ and parameter λ_j.

j	Simplified expression of Φ_j	(m,n)	$\lambda_j(12)$
1	$\phi_1(x)\phi_1(y)$	(1,1)	35.99
2	$\phi_1(x)\phi_2(y)$	(1,2)	73.41
3	$\phi_2(x)\phi_2(y)$	(2,2)	108.27
4	$\phi_1(x)\phi_3(y)$-$\phi_3(x)\phi_1(y)$	(1,3)-(3,1)	131.64
5	$\phi_1(x)\phi_3(y)+\phi_3(x)\phi_1(y)$ $+0.1267\phi_3(x)\phi_3(y)$	(1,3)+(3,1)	132.25
6	$\phi_3(x)\phi_2(y)$	(3,2)	165.15
7	$\phi_3(x)\phi_3(y)$	(3,3)	220.9

After substituting Eq. (11) into Eqs. (9) and (10), multiplying both sides by $\Phi_{j'}(x,y)$, and integrating the expressions over the surface of the plates according to the orthogonality property of the modes, results in

$$M_1\Gamma_j(\omega_j^2-\omega^2)a_j = 2A\beta_{j,00} - 2\sum_{r=0}^{N_r}\sum_{s=0}^{N_s} b_{rs}\beta_{j,rs}, \tag{16}$$

$$M_2\Gamma_j(\Omega_j^2-\omega^2)T_j = 2\sum_{r=0}^{N_r}\sum_{s=0}^{N_s} c_{rs}\beta_{j,rs}e^{ik_z q}, \tag{17}$$

where

$$\Gamma_j = \frac{1}{L^2}\int_0^L \Phi_j^2(x,y)dxdy, \tag{18}$$

$$\beta_{j,rs} = \frac{1}{L^2}\int_0^L \int_0^L \cos(\frac{\pi r x}{L})\cos(\frac{\pi s y}{L})\Phi_j(x,y)dxdy\,. \tag{19}$$

Multiplying both sides of Eqs. (5) and (6) by $\cos(\pi r' x/L)\cos(\pi s' y/L)$, and integrating the expressions over the surface of the plates leads to

$$k_z(b_{rs} - c_{rs})I_r I_s = i\rho\omega^2 \sum_{j=1}^{\infty} a_j \beta_{j,rs}\,, \tag{20}$$

$$k_z(b_{rs}e^{-ik_z q} - c_{rs}e^{ik_z q})I_r I_s = i\rho\omega^2 \sum_{j=1}^{\infty} T_j \beta_{j,rs}\,, \tag{21}$$

where

$$I_r = \frac{1}{L}\int_0^L \cos^2(\frac{\pi r x}{L})dx = \begin{cases} 1/2 & when \quad r \geq 1 \\ 1 & when \quad r = 0 \end{cases}. \tag{22}$$

Equations (16), (17), (20), and (21) form a matrix equation for $[a_j]$, $[T_j]$, $[b_{rs}]$, and $[c_{rs}]$.

Sound power can be obtained by integration of the sound intensity over the plate. Input sound power is given by

$$W_1 = \frac{|A|^2 L^2}{2\rho c}\,. \tag{23}$$

Sound power generated by the radiation due to vibration of the plate is given by

$$W_2 = \frac{1}{2}\int_0^L \int_0^L \frac{k_z}{\rho\omega}|p_t|^2\, dxdy\,. \tag{24}$$

Substituting Eq. (3) into Eq. (24) gives

$$W_2 = \frac{L^2}{2\rho\omega}\sum_{r=0}^{N_r}\sum_{s=0}^{N_s} k_z I_r I_s |d_{rs}|^2\,. \tag{25}$$

The sound transmission coefficient τ is defined as the ratio of transmitted power to incident power as

$$\tau = \frac{W_2}{W_1} = \frac{1}{|A|^2}\sum_{r=0}^{N_r}\sum_{s=0}^{N_s}(\frac{k_z}{k})I_r I_s |d_{rs}|^2\,. \tag{26}$$

STL is defined as

$$\mathrm{STL} = 10\log(1/\tau)\,. \tag{27}$$

3. LOW FREQUENCY APPROXIMATION OF THE STL

In wave propagation through a duct, there exists a cut-off frequency above which waves cannot propagate. It is assumed that the cut-off frequency is low enough such that only $r = s = 0$ (or $N_r = N_s = 0$) is allowed in Eq. (1). Then, in Eqs. (2) and (22), it becomes that $k_z = k$, $I_0 = 1$. Substituting $N_r = N_s = 0$ into Eqs. (16), (17), (20), and (21) yields

$$M_1\Gamma_j(\omega_j^2 - \omega^2)a_j = 2\beta_{j,00}(A - b_{00})\,, \tag{28}$$

$$M_2\Gamma_j(\Omega_j^2 - \omega^2)T_j = 2\beta_{j,00}c_{00}e^{ikq}\,, \tag{29}$$

$$b_{00} - c_{00} = \sum_{j=1}^{\infty} i\rho c\omega\beta_{j,00}a_j\,, \tag{30}$$

$$b_{00}e^{-ikq} - c_{00}e^{ikq} = \sum_{j=1}^{\infty} i\rho c\omega\beta_{j,00}T_j\,. \tag{31}$$

In Eqs. (28)-(31), only symmetric modes are included, since $\beta_{j,00}$ vanishes for anti-symmetric modes according to the definition of $\beta_{j,00}$ in Eq. (19). Note that $\beta_{4,00}=0$ according to Table 2, which shows that the 4th mode is not included in Eqs. (28)-(31) even though it is a symmetric mode. Elimination of a_j and T_j in Eqs. (28)-(31) leads to two equations for b_{00} and c_{00}, and the solutions are

$$b_{00}/A=\alpha_1(1+\alpha_2)e^{ikq}/\Delta, \tag{32}$$

$$c_{00}/A=\alpha_1 e^{-ikq}/\Delta, \tag{33}$$

where

$$\alpha_1=\sum_j \frac{2i\rho c\omega\beta_{j,00}^2}{M_1\Gamma_j(\omega_j^2-\omega^2)}, \tag{34}$$

$$\alpha_2=\sum_j \frac{2i\rho c\omega\beta_{j,00}^2}{M_2\Gamma_j(\Omega_j^2-\omega^2)}, \tag{35}$$

$$\Delta=(1+\alpha_1)(1+\alpha_2)e^{ikq}-e^{-ikq}. \tag{36}$$

The sound transmission coefficient τ in Eq. (26) becomes

$$\tau=|d_{00}/A|^2=|b_{00}-c_{00}e^{2ikq}/A|^2=|\alpha_1\alpha_2/\Delta|^2. \tag{37}$$

Equations (32)-(35) are derived for clamped plates. When the plates are simply supported, mode shape can be expressed as the product of the beam modes as in Eq. (11). Eq. (37) is still valid for simply supported plates, except that α_1 and α_2 are changed by double summations

$$\alpha_1=\sum_m\sum_n \frac{2i\rho c\omega J_m^2J_n^2}{M_1Y_mY_n(\omega_{mn}^2-\omega^2)}, \tag{38}$$

$$\alpha_2=\sum_m\sum_n \frac{2i\rho c\omega J_m^2J_n^2}{M_2Y_mY_n(\Omega_{mn}^2-\omega^2)}, \tag{39}$$

where ω_{mn} and Ω_{mn} are the natural frequencies of the (m,n) mode of plates 1 and 2 defined in Eq. (12). The parameters Y_m and J_m for a simply supported plate are

$$Y_m=1/2, \qquad J_m=\frac{\{1-(-1)^m\}}{m\pi}. \tag{40}$$

The STL of a single plate in a rigid duct can be determined by keeping the terms related to plate 1 in Eqs. (28)-(31). For a clamped plate, Eq. (37) becomes

$$\tau=|b_{00}/A|^2=|\alpha_1/1+\alpha_1|^2, \tag{41}$$

where α_1 is defined in Eq. (34). For a simply supported plate, α_1 in Eq. (38) should be used. From Eq. (41), it is observed that the STL shows peaks when $\alpha_1=0$. On the other hand, when $\omega=\omega_j$ or $\omega=\omega_{mn}$, $1/\alpha_1$ becomes zero, at which the STL shows dips (STL=0).

4. NUMERICAL EXAMPLES

For numerical examples, a plywood plate is considered: $L=280$ mm, $\rho_p=860$ kg/m^3, $E/(1-\nu^2)=$ 4.6 GPa, and $\eta=0.001$. The properties for air are: $\rho=1.2$ kg/m^3 and $c=343$ m/s. Figure 2 demonstrates that only one mode is enough to predict the STL around or below the first dip, and the STLs predicted using two, three, and four modes are almost indistinguishable. However, using one mode cannot predict the peak. Figure 3 compares the STL using Eq. (37) with the FEM result, showing excellent agreement. For clamped and simply supported plates, the STLs are compared in Figure 4, when $h_1=h_2=3$ mm. Figure 4 shows that the clamped condition yields a higher STL than the simply supported condition below the first natural frequency. In all numerical examples, except Figure 2, four modes are considered.

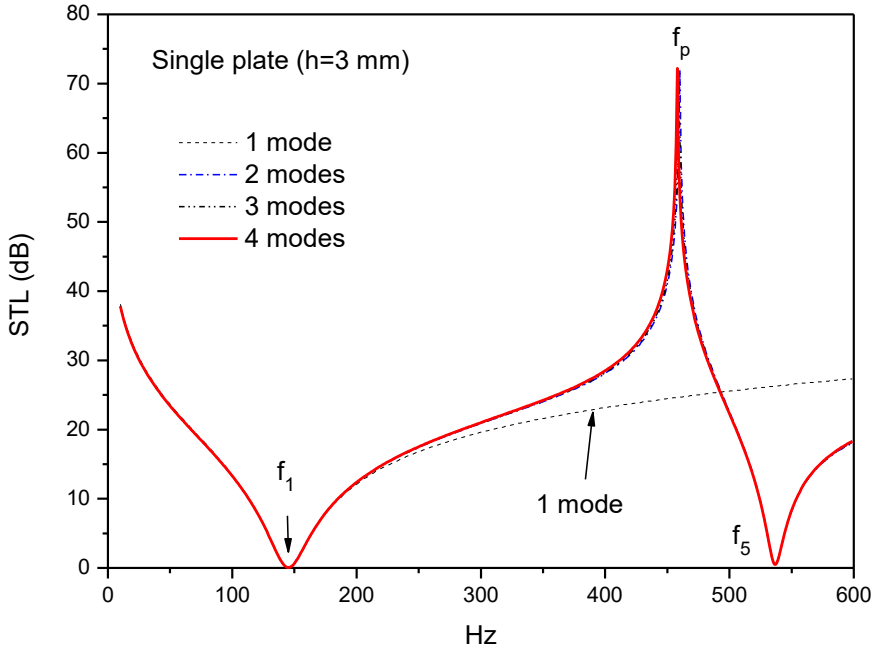

Figure 2. Convergence of the STL of a single plate *vs*. number of the modes when $h_1 = 3$ mm for clamped condition.

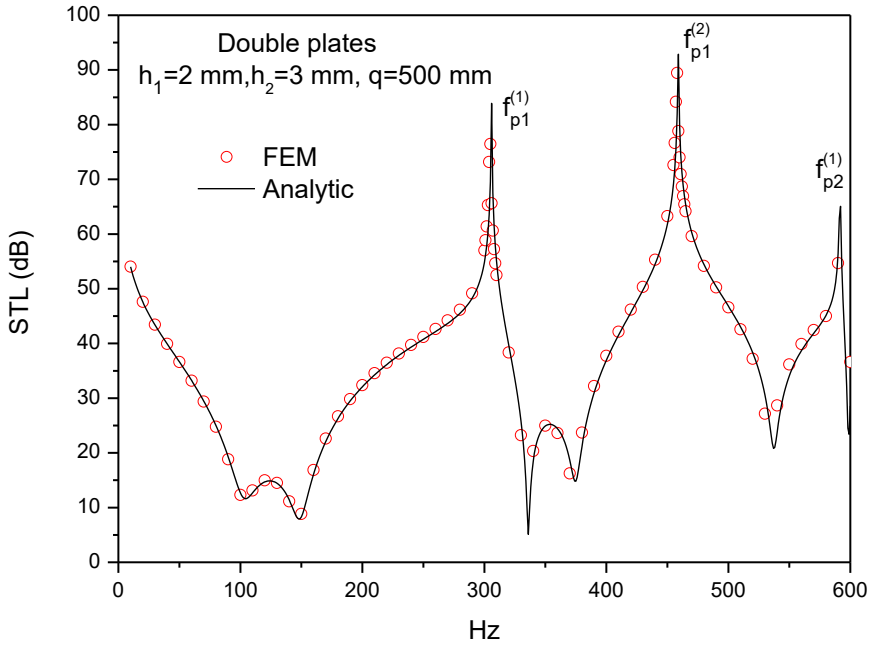

Figure 3. Comparison of the STL of double plates obtained by an analytical method and FEM simulation.

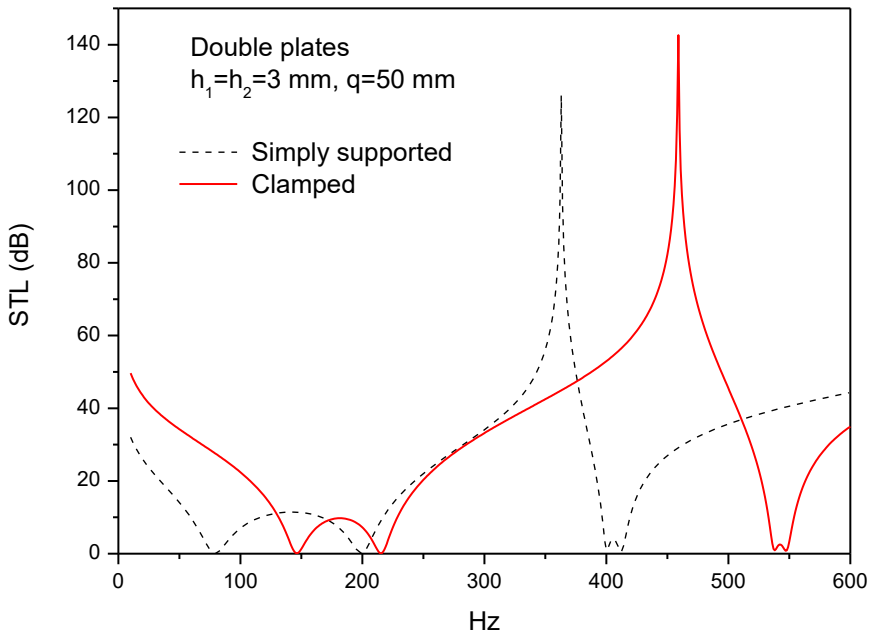

Figure 4. Comparison of the STL of double plates for clamped and simply supported boundary condition. The plate thickness is $h_1 = h_2 = 3$ mm, and distance between plate $q = 50$ mm.

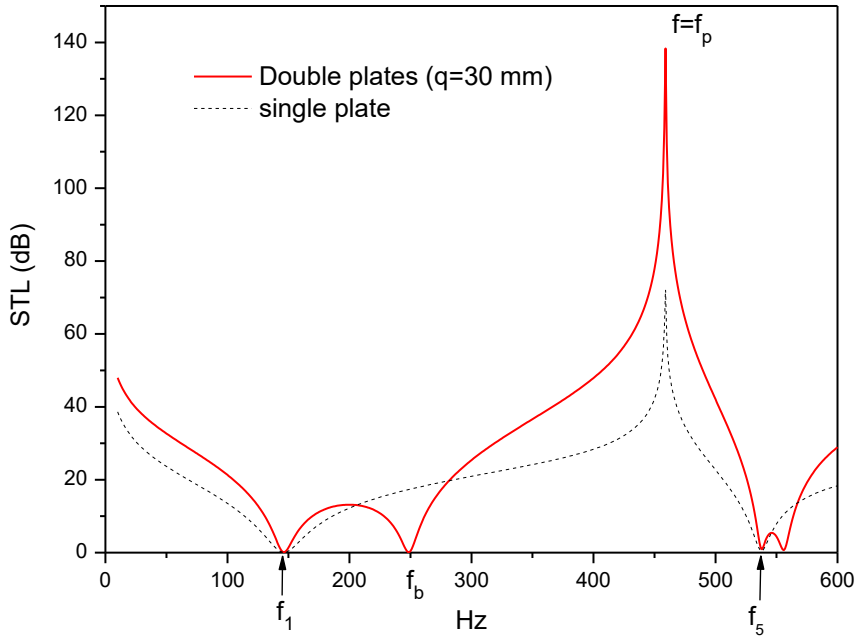

Figure 5. Comparison of the STL of double plates with $h_1 = h_2 = 3$ mm, and $q = 30$ mm, and the STL of a single plate with $h = 3$ mm.

When two plates are identical, Eq. (37) becomes

$$\tau = \frac{1}{\left|(1+1/\alpha_1^2)e^{ikq} - e^{-ikq}/\alpha_1^2\right|^2}. \tag{42}$$

Equation (42) shows that the STL of the double plates becomes zero (or $\tau = 1$) when $1/\alpha_1 = 0$, which corresponds to the dip of a single plate. Figure 5 shows the STL of a single and double plates when $h_1 = h_2 = 3$ mm for clamped condition, where common peaks and dips at the natural frequencies between the single and double plates are found as predicted.

According to Eq. (37), the STL of the double plates has peaks when $\alpha_1 = 0$ or $\alpha_2 = 0$, which corresponds to the peaks of plate 1 or plate 2. In Figure 6, the STL of the double plate with $h_1 =$ 2 mm and $h_2 =$ 3 mm is shown, and STLs of the single plate $h =$ 2 mm and $h = 3$ mm are also plotted. Figure 6 confirms that the peaks of the STL of the double plates coincide with those of the STL of the single plate $h = 2$ mm and $h = 3$ mm

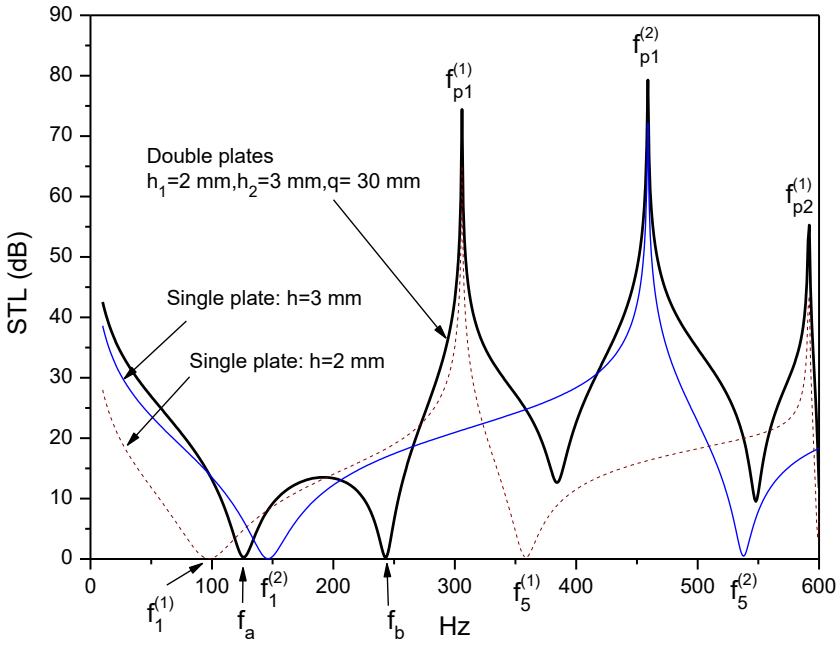

Figure 6. Comparison of the STL of double plates with $h_1 = 2$ mm, $h_2 =$ 3 mm, and $q = 30$ mm, and the STLs of each plate with $h = 2$ mm and $h = 3$ mm. The dips at f_a and f_b are approximately predicted by Eqs. (43) and (44).

The second dip at f_b in Figure 6 corresponds to the plate-cavity-plate resonance (9,10) and its location cannot be predicted analytically. However, when $kq << 1$, approximate location of the dip can be derived. When plates 1 and 2 are not identical, it can be determined that when $kq << 1$, the STL shows dips at the following frequencies, and STL > 0 at the dips

$$\omega_a^2 \approx \frac{(M_1\omega_1^2 + M_2\Omega_1^2)}{(M_1 + M_2)} - q\frac{M_1^2 M_2^2 Y_1^2}{\rho c^2 J_1^4}\frac{(\omega_1^2 - \Omega_1^2)^2}{(M_1 + M_2)^3}, \tag{43}$$

$$\omega_b^2 \approx \frac{1}{q}\frac{(M_1 + M_2)\rho c^2 J_1^4}{M_1 M_2 Y_1^2} + \frac{(M_1\Omega_1^2 + M_2\omega_1^2)}{(M_1 + M_2)}. \tag{44}$$

The solutions (43) and (44) reduce to Eq. (45) when $h_1 = h_2$

$$\omega_a = \omega_1, \quad \omega_b^2 = \frac{1}{q}\frac{2\rho c^2 J_1^4}{M_1 Y_1^2} + \omega_1^2. \tag{45}$$

It is worth noting that the mass-air-mass resonance frequency in an infinite double panel with mass density M_1, M_2 and cavity depth q is given by (46)

$$\omega_0^2 = \frac{1}{q}\frac{(M_1 + M_2)\rho c^2}{M_1 M_2}, \tag{46}$$

which is the same as the first term in Eq. (44) except the term, J_1^4 / Y_1^2, explaining the boundary effect. As q increases, the first dip at $f = f_a$ moves left according to Eq. (43), and the STL increases as shown in Figure 7. The second dip at $f = f_b$ also moves left as q increases as described in Eq. (44).

It should be noted that the STL contains the term of h_1^6 or h_2^6 (recall that $\omega_1^2 \propto h_1^2$ from Eq. (15)). On the other hand, the STL is a function of $\sin kq$ and $\cos kq$. In Figure 7, the STL with increasing q and fixed plate thickness is shown. It may be concluded that increasing the plate thickness affects the STL much more than does increasing the cavity depth q.

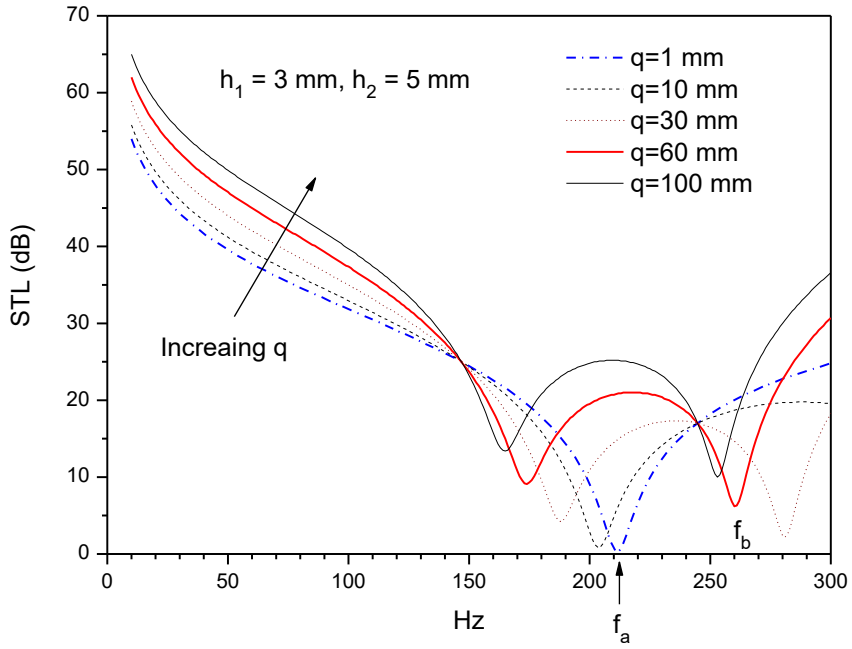

Figure 7. Effect of increasing q on the STL of a double plate while plate thickness is fixed: $h_1 = 2$ mm, $h_2 =$ 3 mm. The first dip frequency f_a moves left as q increases according to Eq. (40).

5. CONCLUSIONS

Under the plane wave assumption, the STL of double plates in a rigid duct was predicted using the first few modes; the accuracy of the proposed method was confirmed by comparison with the FEM result. It was determined that the peak frequencies coincide with those of each plate. When the two plates are identical, the value of STL becomes zero at the natural frequencies of the single plate. It was also shown that inclusion of the first mode of each plate was enough to predict the STL accurately around the first dip. Using a simplified solution, it was possible to investigate how the dips are affected by changing the parameters such as the plate thickness and the cavity depth. Since the STL increases monotonically as the frequency decreases below the first dip, it is important to design the first dip frequency to be sufficiently larger than the target frequency, below which a high STL must be achieved. Hence, making plates more stiffer is essential in achieving high STL at low frequency, such as adding stiffeners on the plate, or making boundary conditions clamped rather than simply supported.

ACKNOWLEDGEMENTS

The present study was supported by the project No. GM3580 and NK198B, “Development of combined technology for low frequency sound absorbing and insulation systems of extreme-material properties” at the Korea Institute of Machinery and Materials.

REFERENCES

1. Fahy F. Sound and Structural Vibration. London, UK: Academic Press Limited; 1985, Chapter 4.
2. Osipov A, Mees P, Vermeir G. Low-frequency airborne sound transmission through single partitions in buildings. Appl. Acoust. 1997; 52(3/4): 273-288.
3. Lee J.-H, J. Kim J. Analysis of sound transmission through periodically stiffened panels by space-harmonic expansion method. J. Sound Vib. 2002;251(2):349-366.
4. Varanasi S, Bolton JS, Siegmund TH, Cipra RJ. The low frequency performance of metamaterial barriers based on cellular structures. Appl. Acoust. 2013;74 :485-495.
5. Piscoya R, Ochmann M. Calculation of the transmission loss of thin plates in a Kundt’s tube. Proceedings of Euronoise 2012, Prague, Czech 2012. p. 560-565.
6. Jessop AM, Li KM, Bolton JS. Reduction of low frequency noise transmitted through a single-pane window. ACTA Acustica United with Acustica. 2011;97:382-390.
7. Kim HS, Kim JS, Kim BK, Lee SH. Low frequency sound transmission of plates in an impedance tube. Proc INTER-NOISE 2015; 9-12 August 2015; San Fransisco, USA 2015.
8. Panneton R, Atalla N. Numerical prediction of sound transmission through finite multilayer systems with poroelastic materials. J. Acoust. Soc. Am. 1996;100(1):346-354.
9. Xin FX, Lu TJ, Chen CQ. Sound transmission through simply supported finite double-panel partitions with enclosed air cavity. J. Vib Acoust. 2010;132: 011008.
10. Xin FX, Lu TJ, Chen CQ. Vibroacoustic behavior of clamp mounted double-panel partition with enclosure air cavity. J. Acoust. Soc. Am. 2008;124(6): 3604-3612.
11. Young D. Vibration of rectangular plates by the Ritz method. J. Appl. Mech. 1950;17:448-453.
12. Leissa AW. Vibration of Plates. New York, USA: Acoustical Society of America; 1993, Chapter 4.